

AD-A259 414

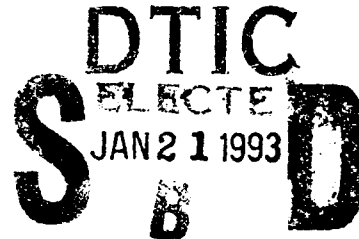
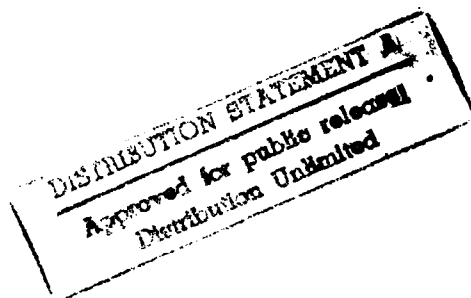


2

**MICROSTRUCTURAL DEVELOPMENT IN A
SPRAY FORMED ALUMINUM-SILICON
CARBIDE BASED METAL MATRIX COMPOSITE**

Second Annual Program Report

Grant No. N0014-91-J-1648



93-00943

**Submitted by
Paul R. Howell
Professor of Metallurgy
The Pennsylvania State University
University Park, PA 16802**

08 1 10 016

FORWARD

This report presents the results which have been obtained in the period January 1, 1992 - December 31, 1992. The experiments were performed primarily by Xiaoli Tang, a graduate student who started on this project in September 1, 1991. Ms. Tang passed her Candidacy Exams for admission to the Ph.D. program in August 1992.

Two papers have been published during 1992:

1. X. Tang, M. H. Tosten and P. R. Howell, "The Precipitation of Plate-Like Phases In Al-Based and Other Alloys", Proc. 3rd International Conference on Aluminum Alloys: Their Physical and Mechanical Properties; Eds. L. Arnberg, O. Lohne, E. Nes and N. Ryum. NTH/SINTEF, 2, (1992), p3 (Appendix I)
2. X. Tang and P. R. Howell, "Microstructural Development of a Spray Formed Aluminum-Lithium/SiC Composite during Aging - A Preliminary Report", Proc. Conf. "American Society for Composites", Technomic Publishing Co. Inc., Lancaster, PA, (1992), p22 (Appendix II)

ABSTRACT

The aging response of an 8090-SiC composite at 190°C has been monitored using microhardness tests, macrohardness tests and transmission electron microscopy (TEM). Intriguingly, it has been found that the composite does not exhibit increased aging kinetics when compared with a control 8090 alloy. Both the control alloy and the composite exhibit a two stage strengthening behavior which is attributed to the precipitation of δ' (Al_3Li) and S' (Al_2CuMg). Quantitative microscopy of the composite has been initiated since it has been found that T2 (Al_6CuLi_3), precipitates on the SiC/matrix interface. Hence, the interfacial area per unit volume (Sv) is of the utmost importance. Finally, the effects of T2 precipitates, at the SiC/matrix interface, on the distribution of δ' have been determined.

DTIC QUALITY INSPECTED 5

per ADA251425	
ADDITIONAL PROCESS	
Dist. Special	
A-1	

1. Measurements of the Aging Kinetics of the 8090 Control Alloy and the 8090-SiC Composite at 190°C

In order to determine the aging response of the 8090-SiC composite, microhardness tests were performed with a load of 10 grams. Special care has been taken to locate the indenter within the matrix away from the SiC particles within the composite. Samples aged up to 30 hours were examined. The results are presented in Fig.1:

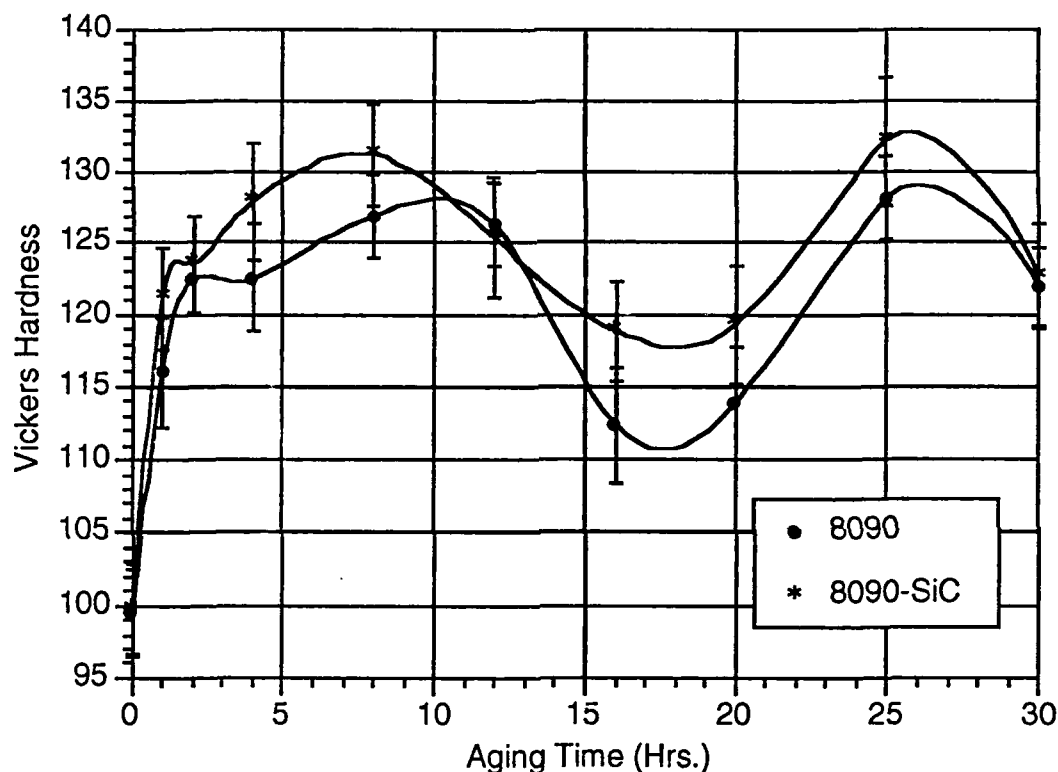


Fig.1 Aging kinetic curves obtained by microhardness measurement

In comparing the aging kinetics of the composite with those of the 8090 control alloy, neither the kinetics nor the peak hardnesses are changed appreciably by the addition of SiC particles. Meanwhile, both materials exhibit a two stage strengthening behavior. It can be expected that the first maximum is due to the hardening effect of $\delta'(\text{Al}_3\text{Li})$ and the second maximum is because of $S'(\text{Al}_2\text{CuMg})$. A more detailed discussion on this point is given in reference [1], which is also appended.

2. Aging Kinetics Represented by the Measurement of the Macrohardness of Both Materials

The macrohardness of both materials has been measured as shown in Fig.2. These measurements were taken to evaluate the mechanical response of the entire material, i.e., the matrix plus the reinforcing SiC particles in the composite. It is unusual that after two hours of aging, the macrohardness does not change appreciably in either material. One exception is a slight decrease in hardness between 10 to 20 hours which corresponds to the hardness minima in the microhardness data (Fig.1). On the other hand, two hours of aging resulted in an obvious strengthening effect when compared with the un-aged samples. These abnormal curves have not been explained as yet and will be the focus of continuing study.

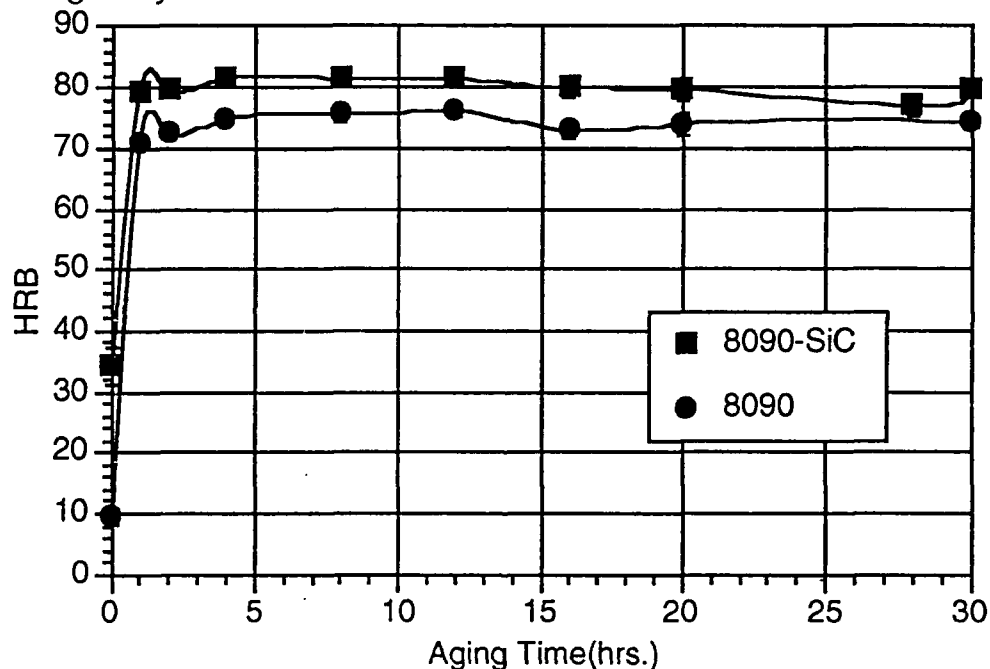


Fig.2 Aging kinetic curves obtained by macrohardness measurement

3. Measurement of the Area of the SiC/Matrix Interface and Grain Boundary Area per Unit Volume

As will be shown in section 4.1.3, T₂ precipitates on the SiC/matrix interface. Hence, it is important to know the interfacial area per unit volume as well as the grain boundary area per unit volume. The specific area of the interfaces and high angle grain boundaries in the matrix have been measured. The specific interfacial area is about $0.3 \mu\text{m}^2/\mu\text{m}^3$ for the SiC/matrix interfaces, and $0.34 \mu\text{m}^2/\mu\text{m}^3$ for the high angle grain boundaries. Hence, the SiC/matrix interfaces may

have a profound influence on microstructural development. In addition, with the assistance of the image scanner, the volume percentage of the SiC particles in the composite has been calculated. The calculated volume percentage of the SiC particles is 16.5% which is close to the 15% claimed by the supplier. Fig. 3 shows the SiC particles and high angle grain boundaries in the matrix.

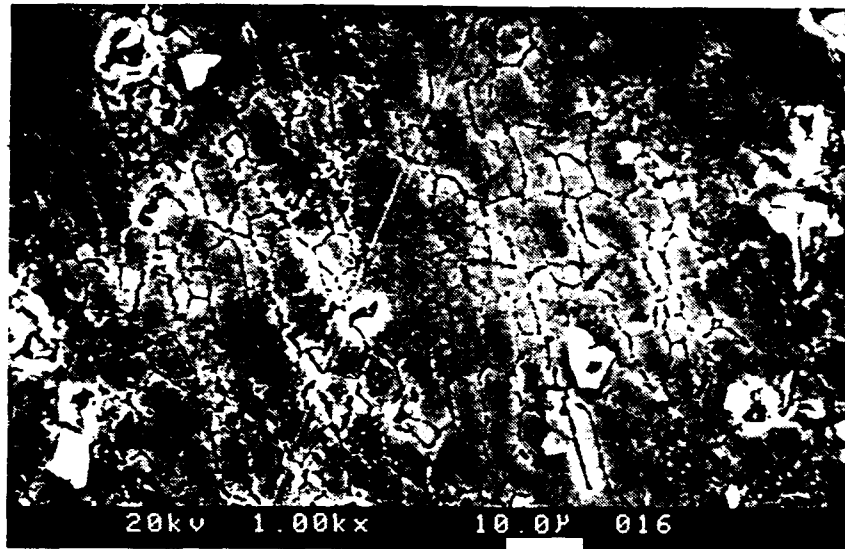


Fig.3 SiC particles and the grain structure of the matrix in the composite

4. Transmission Electron Microscopy Observation of Precipitates in the Control Alloy 8090 and the 8090+SiC Composite

The major focus of this research is on the TEM observation of the microstructural development in both the control alloy and the composite. TEM samples of the control alloy were prepared using a conventional electro-polishing method. The samples were twin-polished in a solution of 30% nitric acid in methanol at about -30°C. This method was very effective for preparing the 8090 control alloy TEM samples. The same procedure failed to produce satisfactory TEM samples for the 8090-SiC composite. The matrix was thinned but the SiC particles were not. Hence, the matrix/SiC interface could not be examined. To make suitable samples of the composite, an ion mill was used. To avoid any possible heating effects during ion milling, on the aging behavior of the composite, a liquid nitrogen cooled, cold stage was used.

Bright field(BF), centered dark field(CDF), and selected area diffraction pattern(SADP) techniques were used in the TEM.

So far, the following observations have been made:

4.1 The Dislocation Distribution in the Composite Matrix

It is well known that a large difference between the thermal expansion coefficient of the matrix and the reinforcement causes a high density of dislocations to be punched out into the matrix of the composite during cooling from e.g., the solution treatment temperature. Therefore, a high dislocation density is a characteristic of the matrix in many composites. As can be seen from the BF image of the matrix shown in Fig.4, the matrix of the composite studied in this research contains a high dislocation density. On the other hand, the dislocation density in the control alloy is quite low as will be seen later. In Fig.4, a BF image, precipitates within the matrix are not visible, due to the strong strain contrast caused by dislocations. Later, we will see that in the 8090 control, the precipitates can be seen quite clearly without the interference of the strain contrast.



Fig.4 High density of dislocations in the matrix of the composite

Because the dislocations are punched out by the reinforcement, they will be distributed in a limited region around the reinforcement, as shown e.g., by Christman and Suresh[2]. Hence, the distribution of the dislocations is not uniform. A highly dislocated region is expected to exist around the SiC particles. In the area far away from the SiC particles, the dislocation density could be lower. Moreover, in the composite used in this research, the distribution of SiC particles is inhomogeneous as shown in the report last year. Hence, a non-uniform distribution of dislocations is expected. This can be appreciated by comparing Fig.5 with Fig.4. Fig.5 is taken from a SiC particle free region. With less interference of dislocation strain contrast, the plate-like S' precipitates can be clearly seen. The above discussion may also go part way to explaining the

apparently abnormal microhardness results, in that the indenter was always placed in region remote from the SiC particles. In order to test this hypothesis, we are writing a proposal to use the nanoindenter at Oak Ridge to obtain Microhardness profiles up to the SiC/matrix interface.



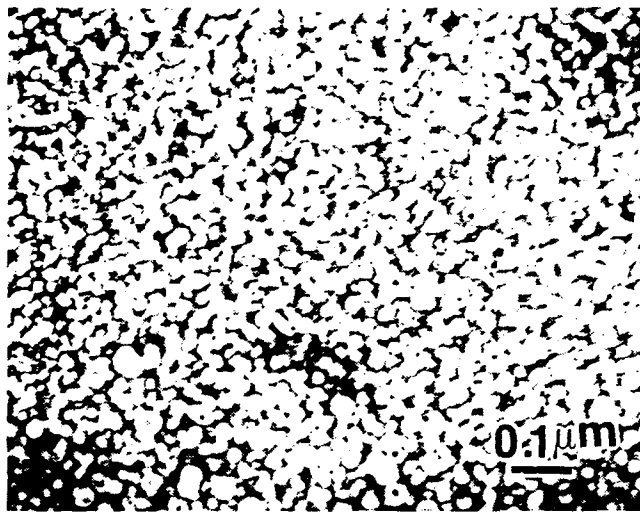
Fig.5 S' precipitates from the composite aged for 25 hrs.

4.2 Precipitates in the control alloy and the matrix of the composite

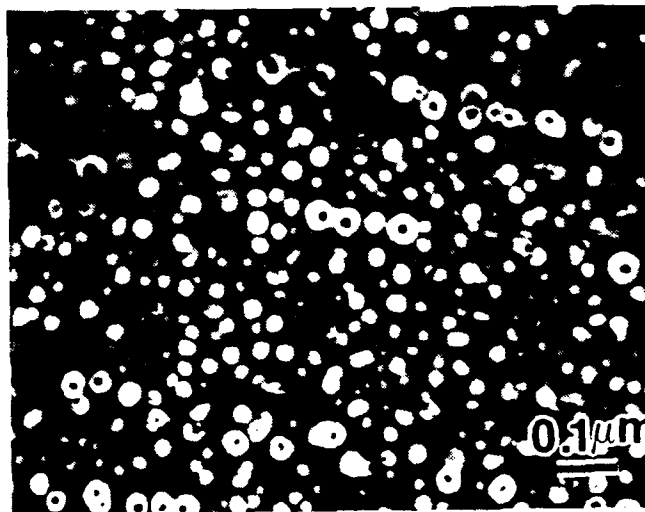
4.2.1 The δ' (Al₃Li) phase

The dominant precipitate species in both materials is δ' (Al₃Li). For the most part, the δ' phase is distributed uniformly in the matrix. Some of them form a duplex structure, enveloping β' (Al₃Zr) precipitates[3].

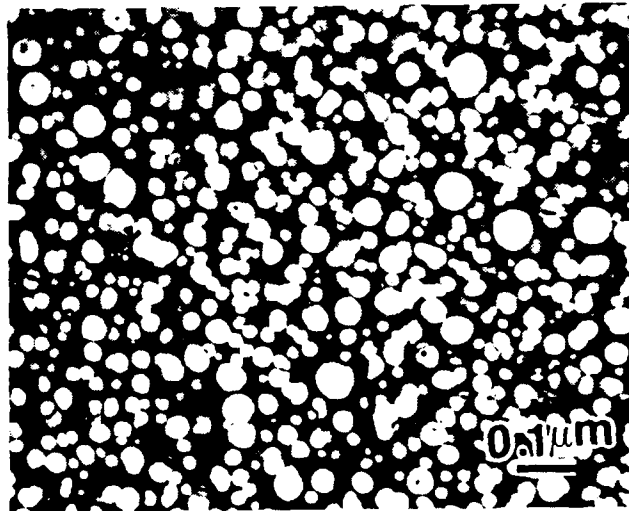
To study the effect of δ' on the aging behavior of the materials, microstructural observations have been related to the aging kinetics. Fig.6(a) is a centered dark field(CDF) image of δ' precipitates in the control alloy, aged for 8 hours. Similar CDF image of δ' precipitates after 20 and 25 hours of aging, are presented in Fig.6(b) and Fig.6(c) respectively. By comparing these images, it can be seen that 8 hours of aging results in finely dispersed δ' precipitates. Longer aging times results in coarsening of δ' precipitates in these materials. Comparing the first microhardness maximum, which occurs at 8 hours aging, with the subsequent drop in microhardness at 20 hours aging, it is clear that finely dispersed δ' precipitates have a powerful strengthening effect in these materials. With coarsening of the δ' precipitates, which occurs as aging time increases, a dramatic drop in the hardening potential of δ' occurs. The coarsening kinetics of the δ' will be determined in the next year, both in the control alloy and the composite.



(a)



(b)

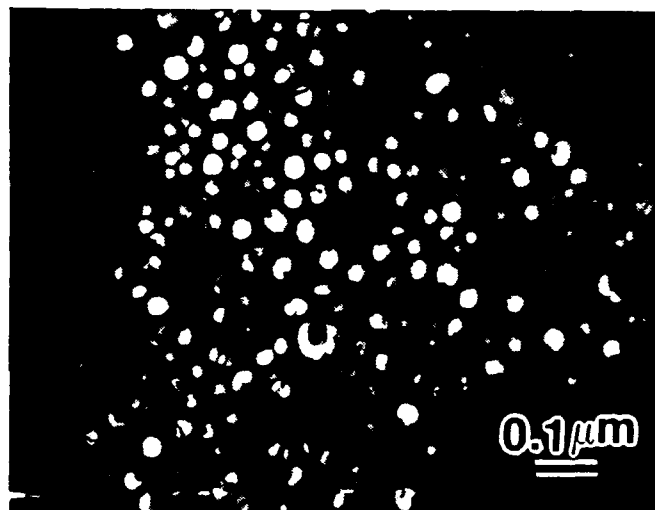


(c)

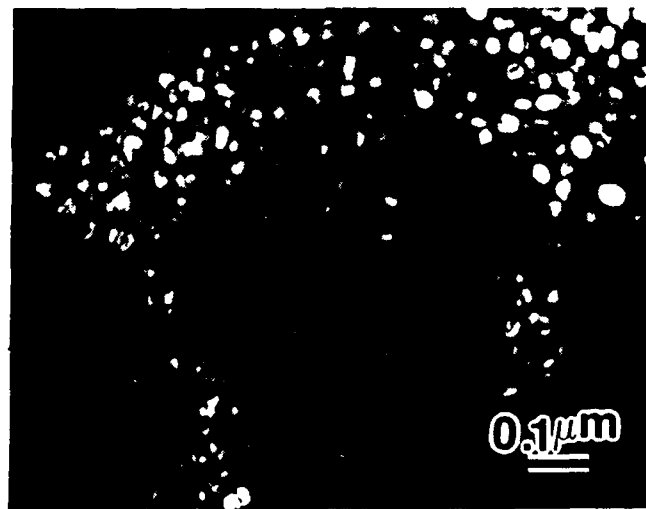
Fig.6 CDF images of δ' in the control alloy((a) 8hrs,(b) 20 hrs and (c) 25 hrs)



(a)



(b)



(c)

Fig.7 CDF image of δ' in the composite((a) 8hrs, (b) 20 hrs and (c) 25 hrs))

All the images shown in Figs.6(a), (b) and (c) are from the control alloy. The distribution and the coarsening process of δ' precipitates in the composite are very similar as can be seen in Fig.7(a), (b) and (c). This is in agreement with the similar aging kinetics between the two materials. Again, quantitative analysis of the composite has been initiated, and will be completed in the next few months.

4.2.2 θ' (Al₂Cu) and S'(Al₂CuMg)

In addition to the δ' and β' phases, θ' and S' have also been identified. Fig.8 and Fig.9 are a selected area diffraction pattern (SADP) from the control alloy and the corresponding θ' CDF image. From the pattern in Fig.8, streaks in the [010] and [001] directions are clearly visible.

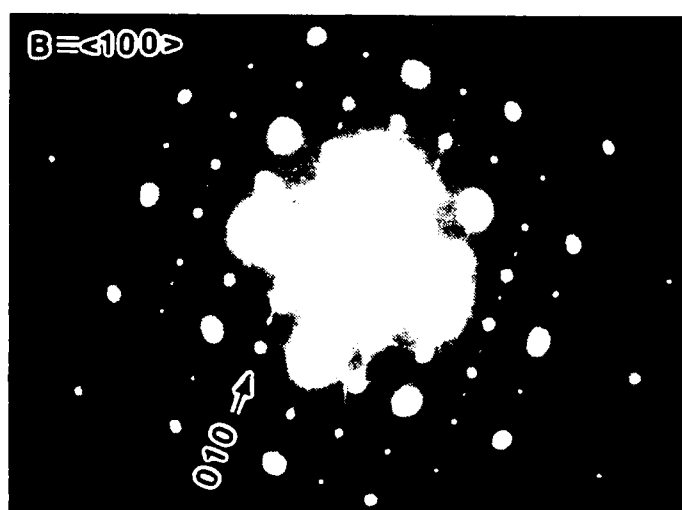


Fig.8 SADP([100] beam direction) from the control alloy aged for 20 hrs



Fig.9 CDF image of plate-like precipitates formed from the pattern shown above

Previous research [4] indicated that in Al-Cu alloys containing Mg, S' could be formed after longer aging times. The addition of Mg to Al-Li-Cu alloys is known to cause a two stage strengthening behavior [5,6]. This phenomenon has also been observed in the current research as shown in Fig.1. The BF image of numerous corrugated S' precipitates in Fig.10 is taken from a control alloy sample aged for 20 hours. Corrugated S' precipitates were first documented by Partridge and Wilson [4]. Fig.11 is a SADP taken from the area shown in Fig.10. From this pattern, streaks in [120] direction can be seen, which is a characteristic of the S' phase. S' precipitates have also been observed in the composite sample as shown in Fig.5 earlier. Fig.5 is taken from the sample after 25 hours of aging. Compared with Fig.10, the precipitate number density is higher in Fig.5. However, the distribution of S' is irregular. An attempt to measure the volume

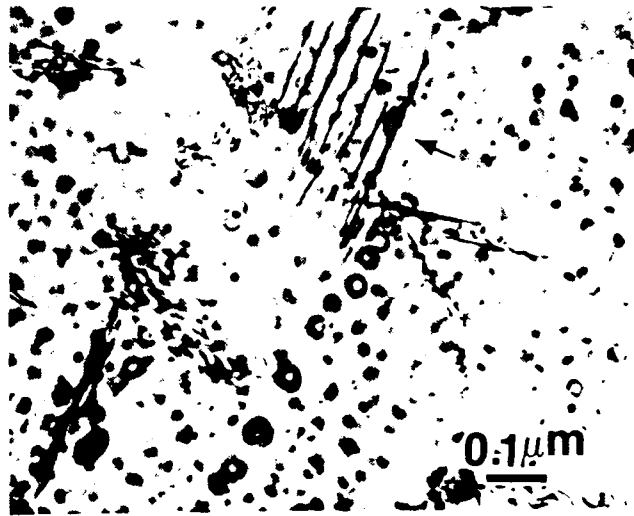


Fig.10 Corrugated plate-like precipitates in the control alloy(20 hrs. of aging)

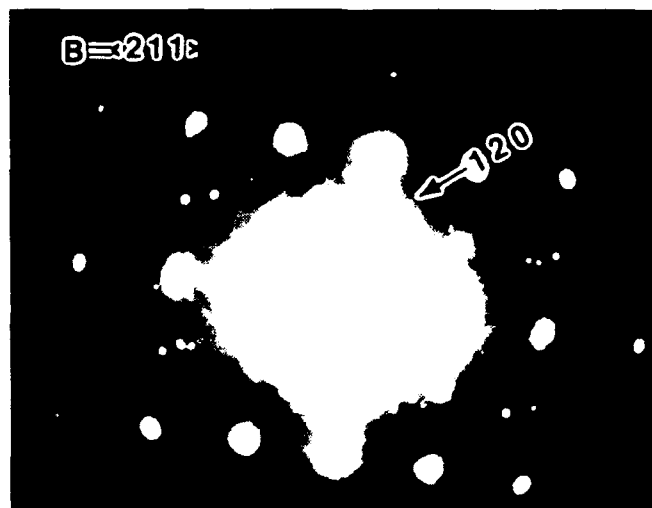


Fig.11 SADP from the area shown in Fig.10

fraction of S' in both the control alloy and the composite is currently underway. Considering that the second hardness peak in the aging kinetic curves occurred at 25 hours of aging, it is believed that S' is the source of this strengthening effect. This conclusion is consistent with previous results[5,6].

4.1.3 T₂(Al₆CuLi₃) phase

In many Al-Li-Cu based alloys, T₂ is an equilibrium phase which forms after relatively long aging times. The nature of T₂ has been extensively studied in previous research[e.g., 7, 8]. T₂ nucleates preferentially at high angle boundaries but also within the matrix as shown in Fig.12. The addition of SiC particles in the composites introduces a lot of interfaces. Using Classical Nucleation theory[9](and see Appendix III), we have shown that these interfaces, which are similar to high angle boundaries, should provide preferential nucleation sites for T₂. Therefore, in the composite, T₂ can be expected to form at the SiC/matrix interface. This has been verified by TEM observation as shown in Fig.13. T₂ is a deleterious precipitate in Al-Li alloys. T₂'s effect on the properties of Al-Li alloys is not only limited to the brittleness of T₂, but also the distribution of other precipitates and dislocations in the composite. This is discussed in the following paragraphs. At this point, our analyses also show that S' would not be expected to form at either high angle grain boundaries or at the SiC/matrix interface (and see Appendix III). Indeed, no evidence for S' precipitation at these interface has been obtained. However, Mahon et al.[10] did find S' at the SiC/matrix interface in a 2124 Al/SiC composite. The reason for the two different findings are currently being sought.



Fig.12 T₂ phase within the grain in the control alloy

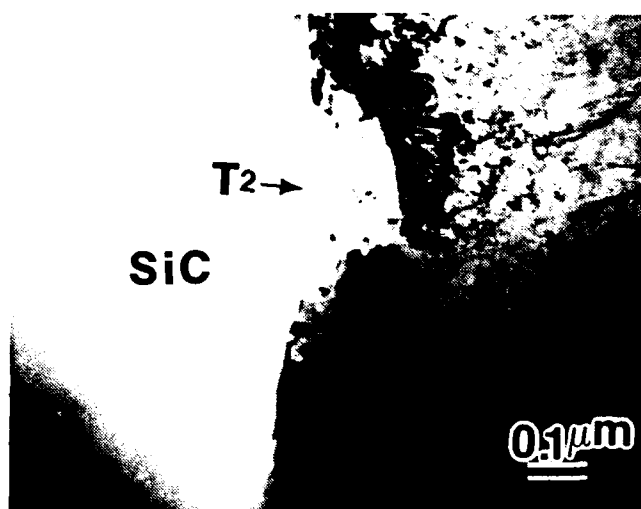


Fig.13 T2 phase at the SiC/matrix interface

4.3 The Effect of the T2 Phase on the Microstructure

4.3.1 δ' precipitate free zones (PFZs) along the high angle boundaries in the control alloy

As mentioned above, T2 is a brittle phase. With the precipitation of T2 at high angle boundaries, the fracture toughness of the material will decrease. Meanwhile, because one of the major strengthening precipitate δ' is a metastable phase containing Li, δ' will be consumed to provide lithium for the formation of the equilibrium phase, T2. Consequently, a δ' PFZ is usually observed along high angle boundaries as shown in Fig.14. Because δ' is a major strengthening phase in this alloy, with the emergence of T2 and the associated δ' PFZ, the grain

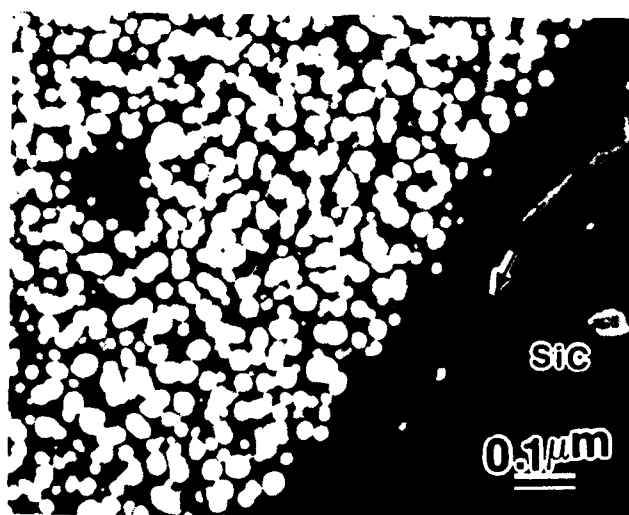


Fig.14 δ' PFZ in the control alloy(after 20 hrs. of aging)

boundary region will be weakened. Hence the strength and fracture resistance of the material will be decreased. Note that δ' PFZs can also develop within the matrix.

4.3.2 T₂ phase and associated δ' PFZs at the SiC/matrix interface

As demonstrated in Appendix II and analyzed in Appendix III (reference [9]), SiC/matrix interfaces are powerful sites for the preferential nucleation of T₂. This analysis has been verified by observation in the TEM. Fig.15(a) is a BF image from the area containing a portion of SiC/matrix interface in a composite sample aged for 20 hours. Some T₂ precipitates with microcrystalline characteristics can be seen at the interface. The microcrystalline nature of T₂ has been discussed at length in reference[8]. To observe the effect of these T₂ precipitates on the



Fig.15(a) T₂ precipitates at the SiC/matrix interface(20 hrs. of aging)



Fig.15(b) δ' PFZ at the SiC/matrix interface(arrowed) shown above

distribution of the strengthening precipitates, CDF images were obtained. A δ' CDF image from the same area as that shown in Fig.15(a) is presented in Fig.15(b). An obvious δ' PFZ exists in the matrix in the vicinity of the matrix/SiC interface. By comparing the CDF micrograph with the BF image in Fig.1, it is clear that precipitation of T2 caused this δ' PFZ.

By further examining the sample aged for 25 hours, T2 precipitates at the matrix/SiC interface are more numerous and coarser as shown in Fig.16(a) (arrowed). The CDF image (Fig.16(b)) shows that the δ' PFZ has further developed into a broader area with increased aging time. The variation of δ' PFZ width with time will be measured in the coming year.



Fig.16(a) T2 (arrowed) phase at the SiC/matrix interface (25 hrs. of aging)

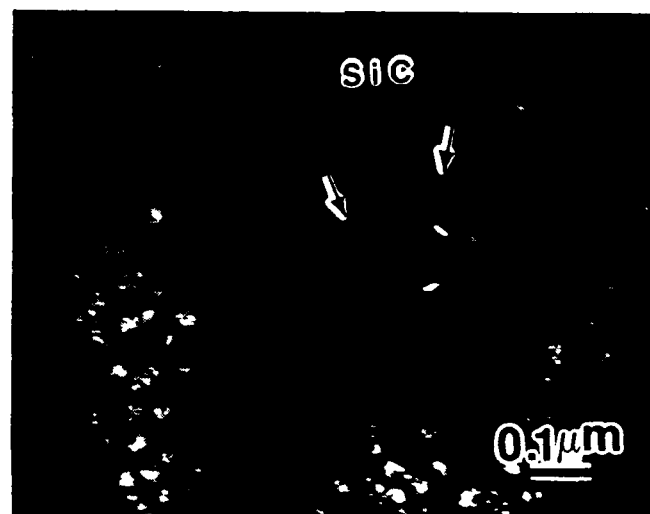


Fig.16(b) A broader δ' PFZ after longer (25hrs.) aging time (interface is arrowed)

If one examines the precipitate distribution in Fig.16(a) carefully, some plate-like precipitates, which are S' , can be seen in the area which has been identified as a δ' PFZ in Fig.16(b). Therefore, it seems that T2 causes δ' PFZ's but does not change the S' distribution.

Although the SiC/matrix interface can be a preferential site for T2 nucleation, T2 does not decorate all SiC/matrix interfaces. As shown in Fig.17, even after 25 hours of aging, δ' can still extend uniformly up to the SiC/matrix interface with no δ' PFZ at the interface.



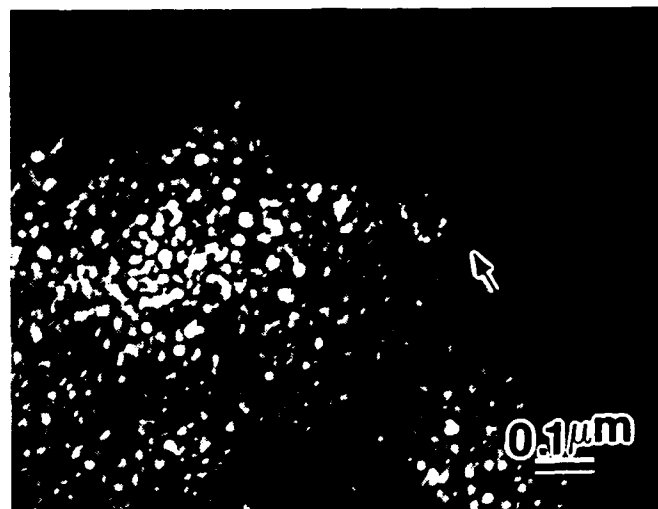
Fig.17 Uniform distribution of δ' in the region around SiC particles

Because the precipitation of T2 and the development of δ' PFZ's are time dependent, and T2 precipitates did not develop uniformly at SiC/matrix interfaces, even after 25 hours, it is of interest to see what happens in samples aged for shorter times. Fig.18(a) and Fig.18(b) are micrographs taken from the samples aged for 8 hours. Compared with the matrix/SiC interface after 20 hours(Fig.15) and 25 hours(Fig.16), the matrix/SiC interface in the sample after 8 hours of aging is almost free of precipitates. Only one isolated T2 precipitate can be identified.

With this virtually precipitate free interface, the δ' PFZ has not fully developed. δ' precipitates extend uniformly to the matrix/SiC interface(Fig.18(b)) for most of its length.



(a)



(b)

Fig.18 Interfacial images from the sample aged for 8 hrs.((a) BF, (b) CDF)

4.3.3 Distribution of dislocations next to the SiC/matrix interface

The effect of T2 on the microstructure of the matrix/SiC interface and its vicinity is not limited to the formation of δ' PFZ's. As analyzed and shown earlier, the dislocation density in the matrix of the composite can be very high; especially in the region around SiC particles. However, in Fig.19, in the matrix immediately adjacent to the matrix/SiC interface, there is a zone which is almost free of dislocations. The dislocation free zone in the vicinity of the matrix/SiC interface is an interesting feature in this composite. As mentioned above, the matrix area around the SiC particles should be highly dislocated and the matrix far away

from SiC, should have a lower dislocation density. One explanation for the unusual dislocation free zones around the SiC particles is that the matrix/SiC interface is a sink for dislocations, if dislocations can move to the interface. Because the matrix usually has a high density of precipitates, dislocation flow is difficult. With the development of a δ' PFZ, most of these obstacles have been eliminated. Dislocations then can move much more easily to the matrix/SiC interface and annihilate. Therefore, a dislocation free zone results from the formation of T2 at the matrix/SiC interface, along with its associated δ' PFZ. Currently, we are examining numerous SiC/matrix interfaces to determine how frequently dislocation free zones develop.



Fig.19 The abnormal distribution of dislocations next to the SiC/matrix interface

Based on the observations presented above, it should be noted that with the δ' PFZ and the dislocation free zone next to the SiC/matrix interface, the matrix next to the interface can be very weak. Failure of the material could well start from this region.

Future Work

i) Time dependence of δ' precipitation

More work is needed to understand the development of the δ' precipitation in samples from as-quenched to up to 30 hours of aging. Quantitative TEM observations are needed to further characterize the coarsening of δ' .

ii) The precipitation process of the S' phase

Preliminary results have been obtained indicating that the second microhardness maximum is due to S' precipitation. Not much is known about the development and the distribution of this precipitate in composite materials.. Because S' is a plate-like precipitate, high dislocation densities should promote precipitation of S'. However, in both the control alloy, which has a low dislocation density, and the composite which is characterized by a high dislocation density in the matrix, the second aging peak for both curves appear at almost the same time. This feature may be related to the non-uniform distribution of dislocations. Therefore, more observations of the development and distribution of S' need to be performed. The distribution of S' will be related to the distribution of the dislocations in the matrix. Nanoindentation profiles should also yield information concerning both the dislocation distribution and the corresponding precipitate distribution.

iii) Dislocation distributions in the composite matrix

As noted earlier, the distribution of dislocations in the composite matrix is non-uniform. In the future study, weak beam(WB) techniques will be used in TEM to get clearer image of the dislocations and their distribution. Based on the results of the dislocation distribution, a complete knowledge about the precipitation and the distribution of plate-like precipitates, e.g. S' and θ' can be obtained. The proper explanation for the aging kinetic curves at 190°C can then be provided.

iv) Development of T2 at the SiC/matrix interface and the associate δ' PFZ's

So far, it has been observed that T2 can be formed after a long aging time and cause associated δ' PFZ's. Not much is known about the kinetics of these phenomena. A complete set of kinetic data is expected, after the systematic measurement on samples aged for different times is completed.

References:

- [1] X. Tang and P. R. Howell, Proc., American Society for Composites, Technomic Publishing Co. Inc., Lancaster, PA, (1992), p22
- [2] M. H. Tosten, J. M. Galbraith and P. R. Howell, J. Mat. Sci. Lett., 6, (1987), p51
- [3] T. Christman, and S. Suresh, Acta. Metall. 36, No.7, 1988, p1691
- [4] R. N. Wilson and P. G. Partridge, Acta Met., 13, (1965), p1321
- [5] K. Welpmann, M. Peters and T. H. Sanders Jr., Proc. 3rd Internation Conf. on Alluminum-Lithium Alloys, eds C. Baler, P. J. Gregoon, S. J. Horris amd C. J. Perf, The Institute of Metals, London, (1986), p525
- [6] S. Song, W. Zhang, J. Cheng, E. R. Ryba, and P. R. Howell, Materials Letters, 2, No.11, July 1990, P430
- [7] M. Audier and P. Guyot, Acta Met., 36, (1988), p1321
- [8] M. H. Tosten, A. Ramani, C-W Bartges, D. F. Michel, E. Ryba and P. R. Howell, Scripta Met., 23, (1989), p829
- [9] X. Tang and P. R. Howell, To be submitted to Scripta Met.
- [10] G. J. Mahon, J. M. Howe and A. K. Vasudevan, Acta Met, et Mat., 38, (1990), p1503

APPENDIX 1

The 3rd. International Conference on Aluminium Alloys: Their Physical and Mechanical Properties. Eds. L. Arnberg, O. Lohne, E. Nes and N. Ryum. NTH/SINTEF, vol. 2, (1992), p.3.

THE PRECIPITATION OF PLATE LIKE PHASES IN Al-BASED AND OTHER ALLOYS

X. Tang* M. H. Tosten** and P. R. Howell*

*Department of Materials Science and Engineering, The Pennsylvania State University,
University Park, PA 16802

**Westinghouse Savannah River Laboratories, Aiken, SC 29808 USA

INTRODUCTION AND BACKGROUND

The nucleation of plate-like phases at grain boundaries had been known to occur for a long time. For example, Vaughan [1] investigated an Al-Cu alloy in detail, and found that θ' formed, predominantly at low angle boundaries and that the number density of precipitates decreased as the angle of misorientation increased. In addition, Vaughan documented a single orientation of θ' on a given segment of boundary and reported that this single variant minimized the angle between the habit plane ($\{001\}_\alpha \parallel \{001\}_{\theta'}$) and the local boundary plane. It was suggested that this orientation formed since it produced the largest reduction in strain energy; a claim that was substantiated by subsequent elastic energy calculations [2]. Aaronson et al., [3] summarized the available data up to (1971) and concluded that for misorientations less than 10° only primary *sideplates* (Widmanstätten plates) formed. Table 1 (modified from reference [3]) lists the systems for which plate like phases had been found to nucleate on low-angle grain boundaries.

Table 1. Systems in which Plate-Like Precipitates form on Low-Angle Grain Boundaries (Modified from [3])		
Alloy	Precipitate	Angular Range
Al-4% Cu	θ' (complex bct)	0-12°
Fe -0.29%C	α (bcc)	-
Al-18% Ag	γ (hcp)	0-17°
Ag-5.6% Al	β (bcc)	0-14°
Al-6.7% Zn -2.5-3% Mg	η' (hcp)	-
Co-20% Fe	α (bcc)	-

In 1975, Lee and Aaronson [4,5] presented a careful mathematical analysis on the effect of faceting on grain boundary precipitation, and showed that as the angle between the habit plane and the grain boundary plane, (\emptyset), decreased, then so did the energy barrier to nucleation (ΔG^*). Figure 1 is a modified version of one of Lee and Aaronson's plots of $\Delta G^*/\Delta G_s^*$ as a function of \emptyset (where ΔG_s^* is the energy barrier for nucleation for an unfaceted allotriomorph). Note that ΔG^* shows a rapid increase with \emptyset , particularly when the relative interfacial energy of the facet (habit plane) is small.

In Lee and Aaronson's papers, the simplifying assumption of ignoring strain energy was invoked, and minimization of interfacial free energy was the major criterion. In (1986), Park and Ardell [6] interpreted their results, on the grain boundary precipitation of the η phase in a commercial Al alloy (7075), in terms of the analyses presented in refs. [4,5]. However, it was also noted in [6] that, for low angle grain boundaries, the η precipitates adopted "well defined plate shaped morphologies."

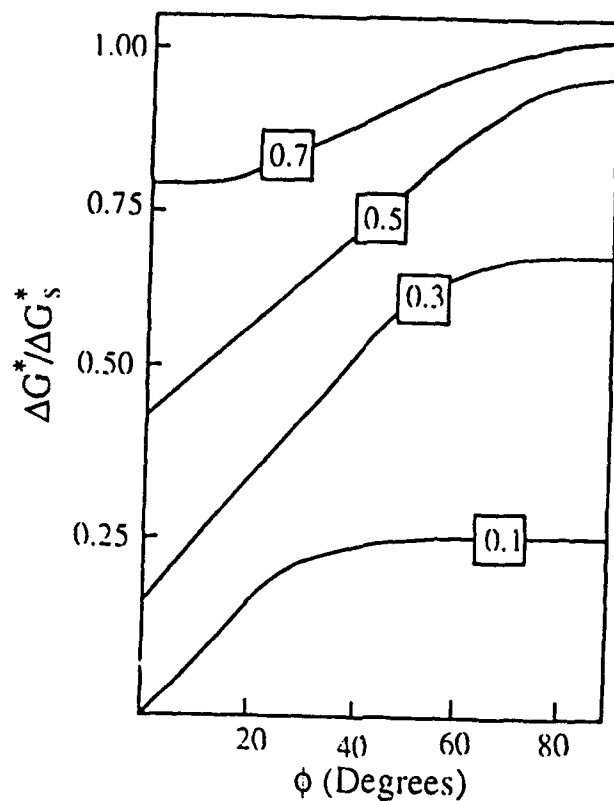


FIG 1. The energy barrier to nucleation for a faceted grain boundary nucleus as a function of ϕ (Adapted from Lee and Aaronson [5]. The four curves are for different values of $\gamma_{\alpha\beta}^c/\gamma_{\alpha\beta}$ where $\gamma_{\alpha\beta}^c$ is the facet energy.

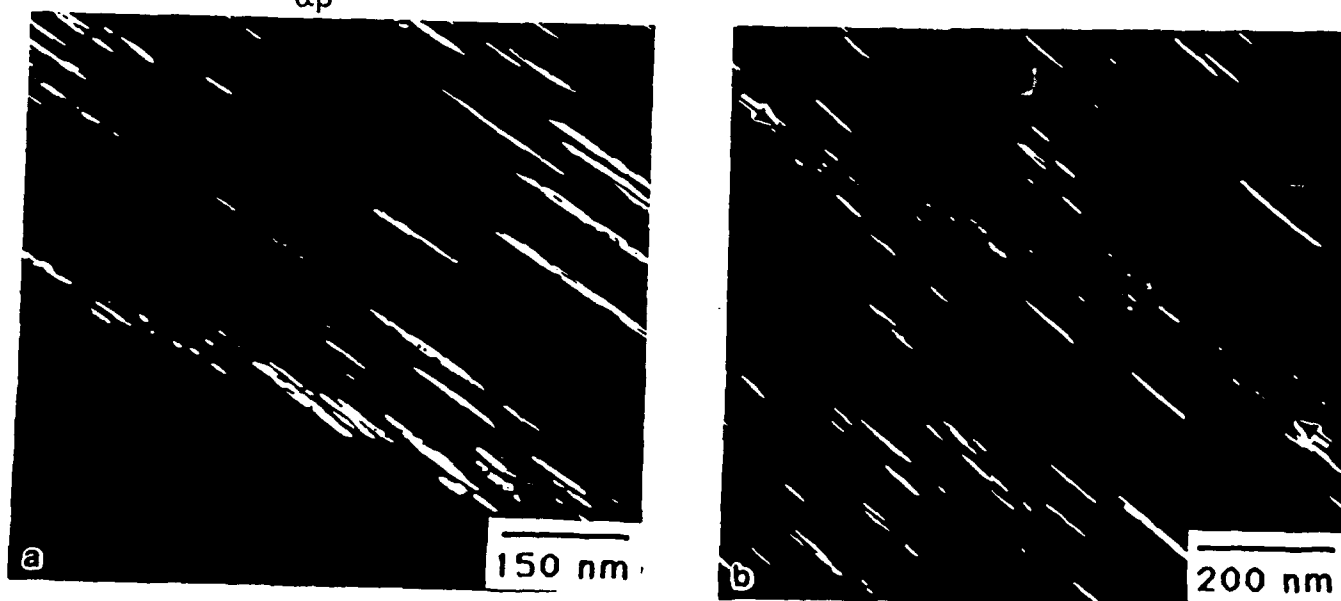


FIG 2. Precipitation of T_1 and θ' on sub-boundaries. a) T_1 centered dark field (CDF) image b) θ' CDF image.

More recently, Luo and Weatherly [7] and Monzen and Kitagawa [8] analyzed the nucleation behavior of b.c.c. precipitates on grain boundaries in an fcc matrix. In both instances, faceting of the precipitates was observed and the habit planes were quoted as:

$$\{121\}_f \parallel \{312\}_b \text{ ref. [7]}$$

$$\{111\}_f \parallel \{110\}_b \text{ ref. [8]}$$

Where the subscripts f and b refer to fcc and bcc respectively. Both studies presented results which were fully consistent with the theoretical predictions of Lee and Aaronson [4.5] in that for general high angle grain boundaries:

- (i) the variant(s) adopted on any given boundary was that which was characterized by the smallest angle between the habit plane and local boundary plane and,
- (ii) as the angle between the low energy facet and the boundary plane increased, the number density of the precipitates decreased.

From the above, it would appear that there are two conflicting viewpoints concerning the efficacy of low and high angle grain boundaries as nucleation sites for plate-like precipitates. The results of e.g., Vaughan [1] show that as the angle of misorientation increases, then the nucleation frequency decreases, whereas the result of e.g., Monzen and Kitagawa [8] show the reverse trend.

In the present paper, grain boundary precipitation of T_1 (Al_2CuLi) and θ' (Al_2Cu), in an Al- 3% Cu- 2% Li- 0.12% Zr alloy, is analyzed. The data will be used to present a rationale for the effect of grain boundary misorientation on the nucleation of plate like precipitates.

EXPERIMENTAL

The experimental alloy, whose composition is given in Table 2, was provided by the Alloy Technology Division of Alcoa Laboratories, Alcoa Center, PA.

Li	Cu	Zr	Fe	Si	Ti	Al
2.1	2.9	0.12	0.06	0.06	0.01	balance

The alloy was solution treated at 550°C for 30 minutes and subsequently aged at 190°C for 120 hours.

Specimens for transmission electron microscopy (TEM) were prepared in a twin-jet electropolisher using a 25% nitric acid -75% methanol solution at -20°C and at an applied potential of about 12V. After perforation, the thin foils were washed in a steady stream of ethanol for one minute and subsequently examined using a Philips EM420T at 120kV.

Grain boundary misorientations were determined using a low camera length, convergent beam electron diffraction (LCL-CBED) technique [9] which employed Kikuchi lines, centers and higher order Laue zones. This technique yields an accuracy of better than 0.5°.

RESULTS

In general, sub-boundaries (arbitrarily defined as $\theta < 1$) were excellent nucleation sites for both T_1 and θ' . Figures 2 a,b are T_1 and θ' centered dark fields (CDFs) respectively and show that there is a high number density of these plate like phases. Reference to figure 2a also shows that the precipitates on the sub-boundaries often tended to be shorter, but thicker than the intragranular precipitates. As the misorientation increased, there was a rapid decline in the number density of

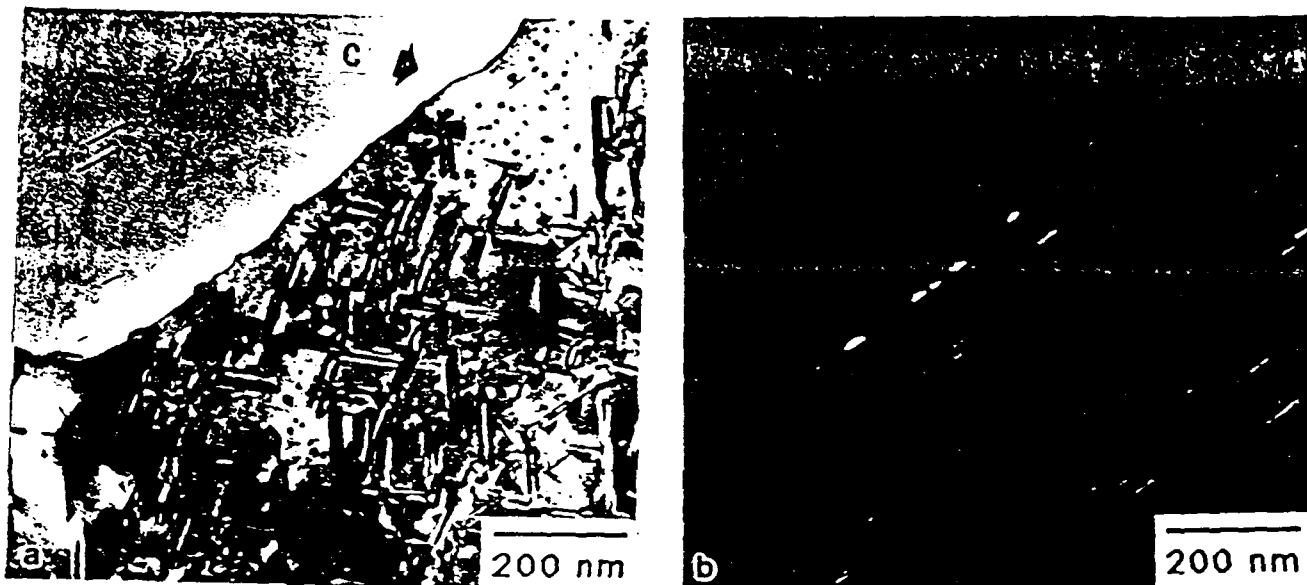


FIG 3. Bright field (BF)/ θ' CDF images of precipitation on a low angle grain boundary. a) BF image. Note the δ' precipitate free zone at C. b) θ' CDF image. Note that the θ' habit plane is at a low angle to the grain boundary plane.

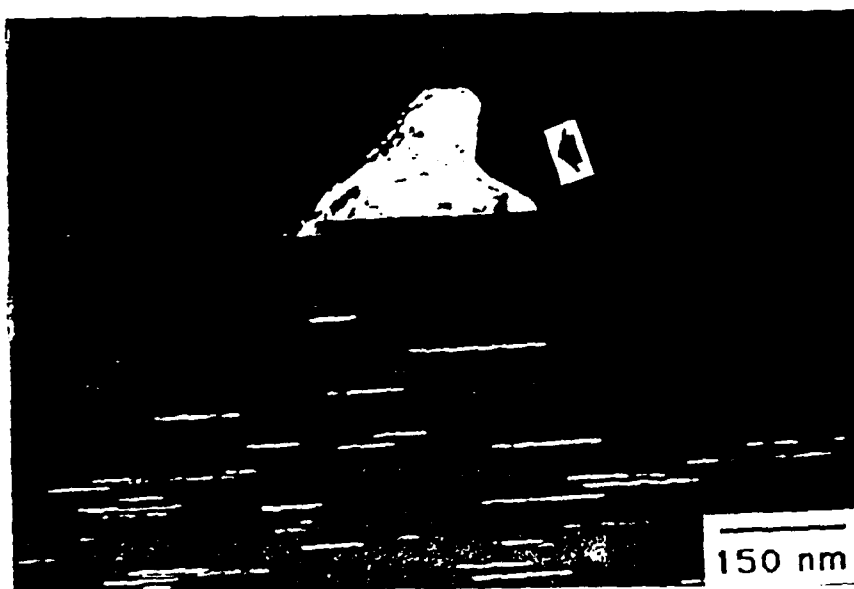


FIG 4. A T_1 precipitate on a triple junction.

both the T_1 and θ' . Figures 3a,b are a bright field/ θ' dark field pair of a low-angle grain boundary for which the misorientation is 6.5° . A δ' precipitate free zone is evident at C. The intergranular θ' are related to the lower, right-hand grain but have grown predominantly into the upper, left-hand grain. This should be contrasted with precipitation on sub-boundaries where growth appeared to occur equally into both grains. Reference to figures 2-3 also shows that the angle between the habit plane and the local boundary plane is low.

T_1 was rarely observed on high angle grain boundaries; one of those occurrences is presented in the T_1 centered dark field image of figure 4. The single T_1 precipitate is located at a triple junction, is related to the lower grain, and has grown smoothly into the other two grains. Finally, figure 5 shows another high angle grain boundary and several T_2 (Al_6CuLi_3) precipitates are arrowed.

DISCUSSION AND SUMMARY

The results of the present investigation are completely in agreement with the earlier investigation of Vaughan and can be explained in exactly the same fashion i.e., nucleation occurs on low angle grain boundaries as opposed to homogeneously, due to the reduction in strain energy, not interfacial energy. Hence, as the angle of misorientation increases, the strain energy of the boundary decreases and the interfacial energy increases. Consequently the nucleation frequency of both θ' and T_1 decreases.

Returning to Park and Ardell's paper [6] they noted that for low angle grain boundaries:

- (i) the number density of η precipitates was high;
- (ii) the η precipitates were plate like;
- (iii) the number density of the η particles decreased as the angle of misorientation increased.

Hence, we propose that the major reason that η precipitates on grain boundaries is due to strain energy considerations, and that interfacial energy only plays a secondary role. This is consistent with the fact that, in common with θ' and T_1 , intragranular nucleation of the η phase occurs on dislocations (see e.g., [10]).

In contrast, we believe that the converse is true for the fcc/bcc systems examined by Luo and Weatherly [7], Monzen and Kitagawa [8], where the complex semicoherent nature of all interfacial orientations, e.g., see [11] would favor high angle grain boundary nucleation. Again, this is consistent with the findings of Monzen and Kitagawa [8] who showed that low angle boundaries were not efficient nucleation sites.

In summary, we believe that, for a second phase particle with a given habit plane, if strain energy in one dimension, perpendicular to the habit plane, is significant enough to hinder the nucleation process, then low angle boundaries will be better nucleation sites than high angle boundaries. Conversely, if strain can be essentially ignored, high angle boundary nucleation will be favored over low angle boundary nucleation.

ACKNOWLEDGMENTS

The authors acknowledge the Office of Naval Research, Grant #N00014-91-J-1648 and the Alloy Technology Division of Alcoa Laboratories, Alcoa Center, PA for financial support.

REFERENCES

- [1] Vaughan, D., Acta Met., 16, p. 563 (1967)

- [2] Simon, J. P. and Guyot P., J. Mat. Sci., 10, p. 1947 (1975)
- [3] Aaronson, H. I., Aaron, H. B and Kinsman, K. R., Metal., 4, p. 1 (1971)
- [4] Lee, J. K. and Aaronson, H. I., Acta Met., 23, p. 799 (1975)
- [5] Lee, J. K. and Aaronson, H. I., Acta Met., 23, p. 809 (1975)
- [6] Park, J. K. and Ardell, A. J. Acta Met., 37, p. 2399 (1986)
- [7] Luo, C. P. and Weatherly, G. C., Acta Met., 37, p. 791 (1989)
- [8] Monzen, R. and Kitagawa K., Scripta Met, 22, p. 173 (1988)
- [9] Parayil T. R., Ph.D. Thesis, The Pennsylvania State University, PA 16802, Pennsylvania, USA, (1986).
- [10] Lorimer, G. W., In: Precipitation Processes in Solids, (K. C. Russell and H. I. Aaronson, eds.), TMS-AME, Warrendale, USA, p. 87 (1978)
- [11] Luo, C. P. and Weatherly, G. E., Acta Met., 35 p. 1963 (1987).

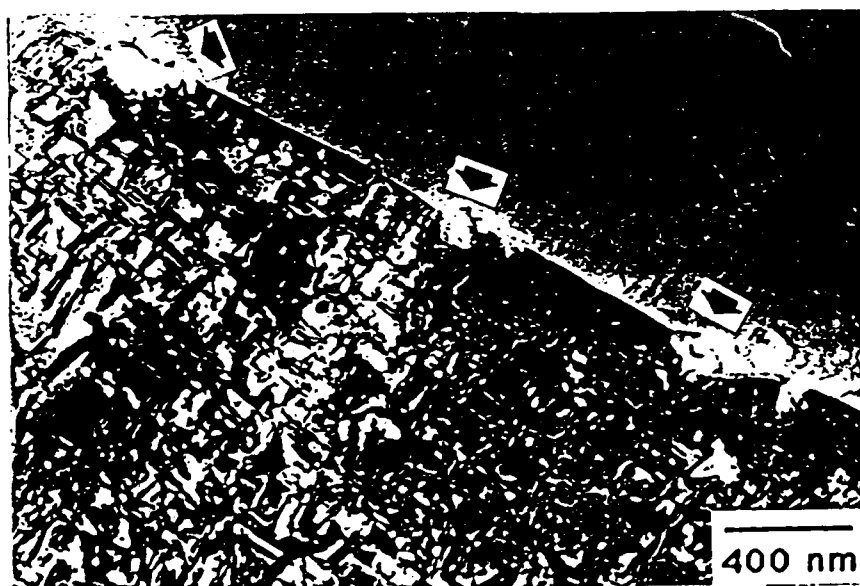


FIG 5. BF image of a typical high angle grain boundary. Only T_2 precipitates (arrowed) are found.

Microstructural Development of a Spray Formed Aluminum Lithium/SiC Composite during Aging— A Preliminary Report

X. TANG AND P. R. HOWELL

ABSTRACT

The microstructure and mechanical properties of an aluminum-lithium/silicon carbide (Al-Li/SiC) spray formed composite have been examined using a combination of scanning electron microscopy (SEM), transmission electron microscopy (TEM) and microhardness measurements. In addition, the behavior of the composite has been compared with a control alloy that was processed in the same fashion as the composite.

Aging at 190°C led to the development of the δ' (Al_3Li) phase in both the composite and control alloy. This yielded a matrix peak hardness after approximately 10 hours. Subsequently, precipitation of the S' (Al_2CuMg) phase yielded a second matrix hardness peak after 25 hours aging. Somewhat intriguingly, both the control alloy and the composite exhibited virtually identical matrix aging behavior.

INTRODUCTION

The aluminum alloy 8090 has been used in numerous applications because of its high strength, excellent resistance to fatigue crack growth and good plane-stress fracture toughness. With the addition of SiC, the strength can be increased further and the density decreased. Hence, an 8090 alloy matrix reinforced with SiC has potential applications in aerospace engineering. However, in order to realize its full potential, it is necessary to understand:

- (i) how the microstructure of the matrix evolves during aging;
- (ii) how the aging process is affected by the presence of the reinforcing particulates, and,
- (iii) how the SiC/aluminum interface modifies the aging response of the matrix.

Therefore, one of the major objectives of the present investigation is to provide a detailed understanding of the microstructural development of a spray formed Al-Li/SiC composite. This has necessitated the use of transmission electron microscopy (TEM) and scanning electron microscopy (SEM). In addition, in order to assess the effects of the SiC particles, an 8090 control alloy was processed in the same fashion and compared with the composite material. Finally, to examine the mechanical properties of the matrix, microhardness measurements have been taken as a function of aging time for both the composite and the control samples.

EXPERIMENTAL

MATERIALS

The composite material used in this study was a spray formed particulate 8090* powder metallurgy aluminum alloy containing about 15% vol. SiC particles. The SiC particle sizes were in the range of 3 - 10 μ m. An alloy without the SiC particles was made using the same processing methods in order to compare the matrix aging behavior with and without the SiC particles. These materials were provided by the Office of Naval Research. Both materials were extruded at 370°C using an extrusion ratio of 17:1. The bulk samples were solution heat treated at 536°C for 45 minutes. An ice water quench was performed upon the removal of samples from the furnace. To observe the aging behavior, samples from both materials were aged at 190°C for up to 30 hours.

MICROHARDNESS TESTS

Microhardness values of both the control alloy and the matrix of the composite were used to indicate property changes that occur during the aging process. The measurements were performed on a LECO M-400 microhardness tester with a 136° Vickers diamond indenter. To ensure that the microhardness values reflect the property of the matrix of the composite, a small load of 10 grams was used to reduce the possibility of the indenter impinging on the SiC particles. Also, the test points were carefully chosen. Because the SiC particles just below the surface of the sample would alter the shape of the indents, only the indents with a regular shape were measured. Some abnormally high hardness values were attributed to the effect of the SiC particles and subsequently ignored. At least 30 microhardness measurements were performed for each sample and the standard deviation was <4.5.

TEM OBSERVATIONS

Samples were cut from the bulk material using a diamond blade. The control alloy samples were mechanically ground to a thickness of 30-40 μ m using 200 to 600 grit SiC paper. The TEM foils were prepared using a twin-jet polisher with 30% nitric acid and 70% methanol solution at <-30°C with a potential of 15V. The composite samples were mechanically ground to a foil thickness of less than 100 μ m using a loose abrasive method. This method involved grinding with a diamond suspension on a woven stainless steel polishing cloth. Circular disks, 3mm in diameter were punched out from the foil and dimpled to about 10 μ m. The foil was then ion milled at 3.5 keV and 0.5mA per gun. A cold stage cooled by liquid nitrogen was used to avoid heating effects caused by the high energy ion bombardment. By choosing the ion beam angle properly, both the matrix and the SiC could be thinned to a satisfactory thickness.

Twin-jet polishing was tried on the composite material. With this method, the matrix of the composite thinned but the SiC particles did not. Because of this abrupt thickness change from the SiC to the matrix, the microstructure of the matrix/SiC interface could not be observed clearly.

TEM observations were performed on Phillips EM420T with a voltage of 100 to 120kV.

* Normal Composition (wt%)

Li	Cu	Mg	Zr	Al
2.25	1.0	0.80	0.12	balance



Fig. 1. SiC distribution and the precipitates at grain boundaries (aged at 190°C for 8 hrs).

RESULTS

SEM EXAMINATION

- An SEM image of the composite, which had been aged for 8 hours, is shown in figure 1. From the micrograph, it can be seen that:
- a) the distribution of the SiC particles is not uniform. Some regions are almost free of SiC particles, other regions contain clusters of SiC;
 - b) the size of the SiC varies. Most of the SiC particles have diameters of about 3-4 μm and are irregular in morphology. In contrast, some elongated ($\approx 10 \mu\text{m}$ in length) particles are also present;
 - c) the aluminum grains are elongated along the extrusion direction and the grain boundaries are seen to be decorated with precipitates. In addition, some of the rod-like SiC particles are oriented parallel to the long axis of the grains.

AGING CURVES AT 190°C

The age hardening response of both the composite and the control alloy are presented in figure 2. From figure 2, it can be seen that:

- a) both materials show a two-stage strengthening behavior with hardness maxima at approximated 7 1/2 hours and 25 hours;
- b) the addition of 15% SiC does not appear to have any appreciable effect on the aging response of the matrix.

In an attempt to explain these two rather unusual results, both the control alloy and the composite have been examined using TEM and the results of our preliminary investigation are given in the following two subsections.

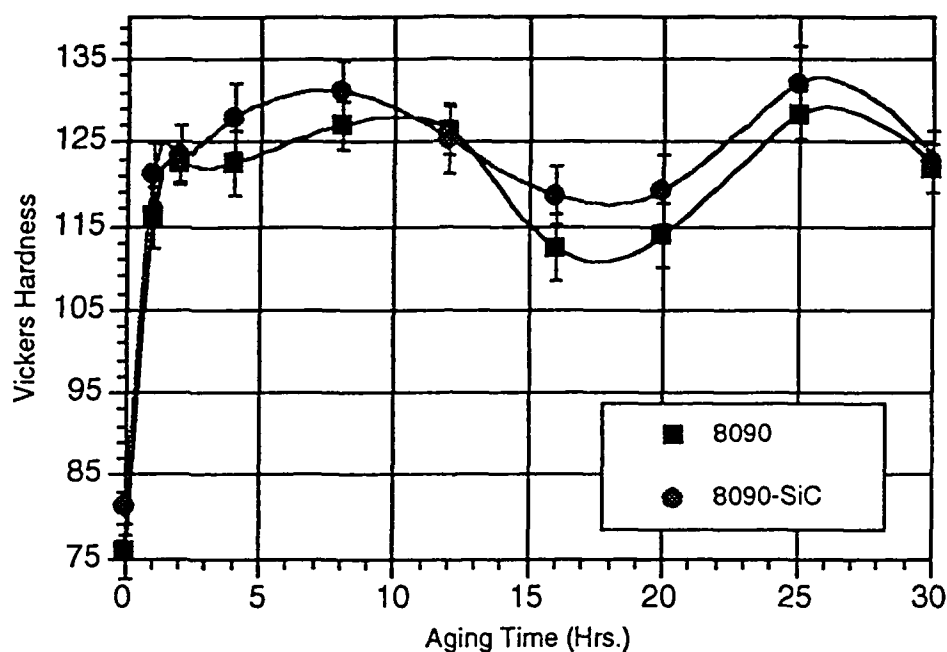


Fig. 2. Aging kinetic curves at 190°C.

A TEM INVESTIGATION OF THE CONTROL ALLOY

In order to investigate the appearance of a double maxima in the hardness data, the control alloy was examined first. Figure 3 is a δ' (Al_3Li) centered dark field (CDF) image of specimen material that had been aged at 190°C for 8 hours. The high number density of δ' yields the first hardness maxima. At this stage, little evidence for S' (Al_2CuMg) was found. Reference to figure 3 shows that the cores of some of the large δ' (e.g., arrowed) are "dark imaging". These cores are, in fact, β' (Al_3Zr) which form during primary processing, and remain essentially unchanged during subsequent thermomechanical processing.

After 20 hours of aging, δ' has coarsened significantly, as can be seen with reference to figures 4a, b (bright field (BF) and δ' CDF images respectively). For this aging time, the δ' is also being partially replaced by the thermodynamically more stable T_2 (Al_6CuLi_3) phase (arrowed on figure 4a). Note that a δ' precipitate free zone (PFZ) develops in the vicinity of the T_2 particle (figure 4b). Figure 5 is also a δ' CDF (20 hours aging) and shows that PFZs develop at high angle grain boundaries (the latter is arrowed on figure 5). Again, it is likely that this PFZ forms due to the precipitation of T_2 on the high angle grain boundaries (see figure 1).

After 20 hours of aging, S' is observed to form in the matrix (arrowed on figure 6a). The S' precipitates on $[210]$ matrix planes, yielding streaks with $\langle 210 \rangle$ directions, as arrowed on the selected area diffraction pattern (SADP) of figure 6b ($[211]$ matrix beam direction).

After 25 hours of aging (corresponding to the second hardness peak), copious precipitation of S' has occurred on all dislocations to produce the characteristic, corrugated dispersions which are seen in the BF image of figure 7.

A PRELIMINARY TEM INVESTIGATION OF THE COMPOSITE

Thus far, the composite has only been examined using TEM after 20 hours of aging. Figures 8a, b are BF images of the composite. In figure 8a, a high dislocation density is

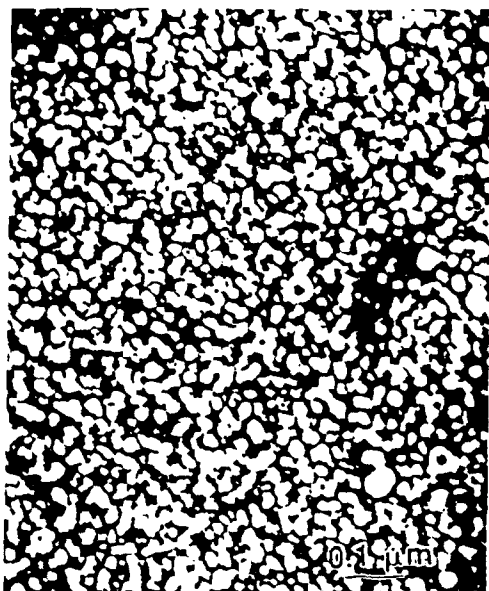


Fig. 3. CDF image of δ' in the control alloy aged at 190°C for 8hrs.

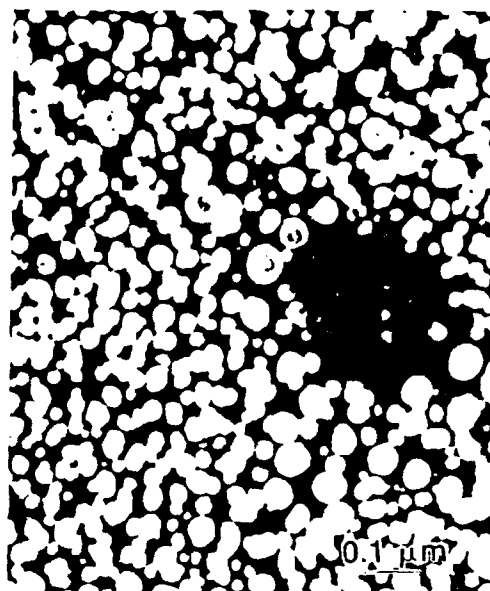


Fig. 4a. CDF image of δ' in the control alloy aged at 190°C for 20 hrs.

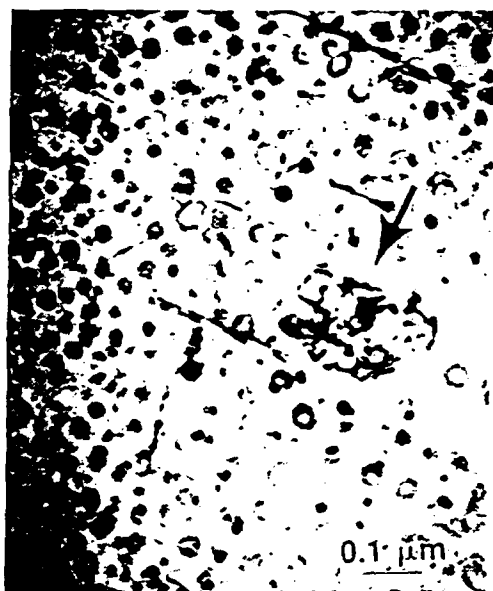


Fig. 4b. BF image of the same region shown in fig. 4a. (T_2 arrowed).

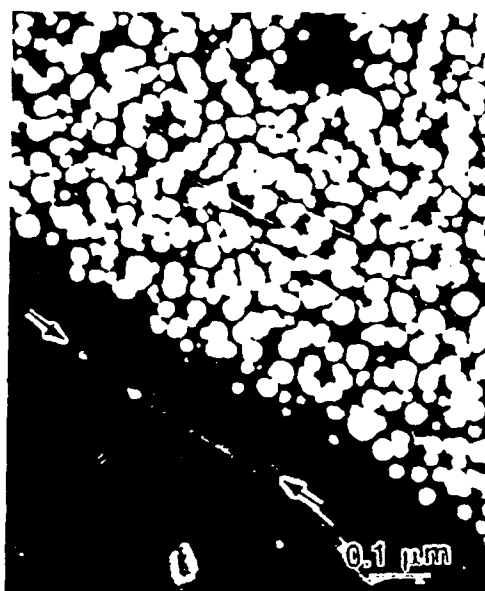


Fig. 5. PFZ of δ' along the high angle boundary (190°C, 20hrs).

observed (e.g., compare figure 8a with figure 7, the latter being recorded from the control alloy). In contrast, a much lower dislocation density is observed in figure 8b. The δ' distribution in the composite was similar to that obtained in the absence of the SiC, as is shown in the δ' CDF of figure 9 from the composite, and in figure 4b from the control.

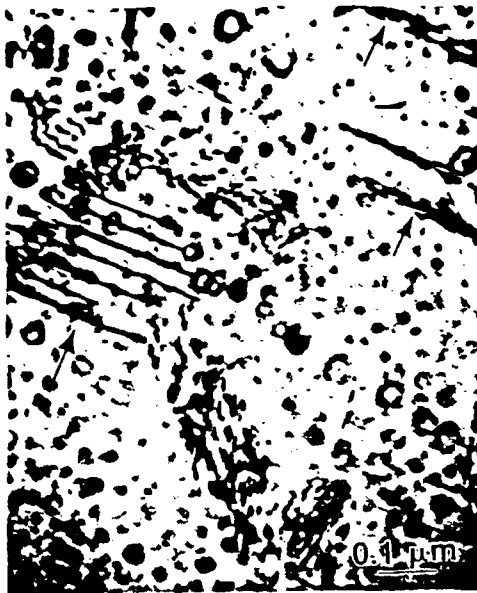


Fig. 6a. BF image of S' in control alloy.

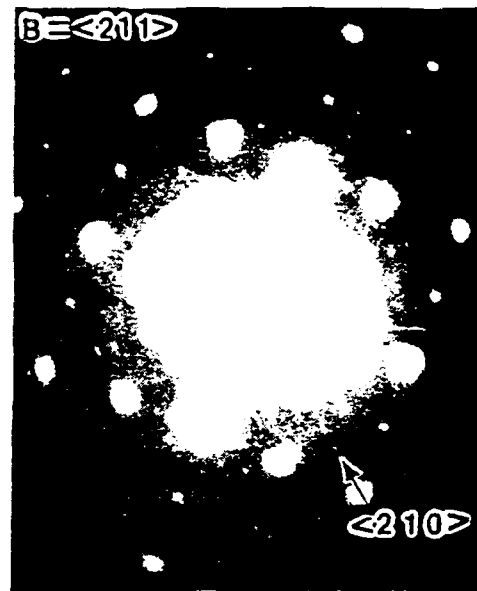


Fig. 6b. Diffraction pattern from the region shown in fig. 6a.



Fig. 7. Dislocations with the corrugated S'.



Fig. 8a. High dislocation density in composite.

THE ALUMINUM/SILICON CARBIDE INTERFACE

Figures 10a, b are a BF/SiC CDF pair (the SiC is so labeled on figures 10a, b). The interface is arrowed A on figure 10a, and it is interesting to note what appears to be a dislocation free zone (DFZ) is located in the immediate vicinity of the interface (arrowed B on figure 10a). However, a high dislocation density is present away from the interface. Reference to figure 10b shows the presence of defects (probably faults) within the



Fig. 8b. A lower dislocation density (compared to fig. 8a).

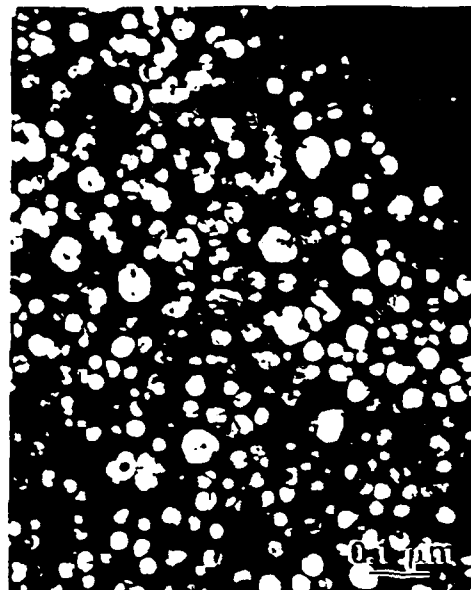


Fig. 9. CDF image of the δ' in the composite (190°C, 20hrs).



Fig. 10a. BF image of matrix/SiC interface.

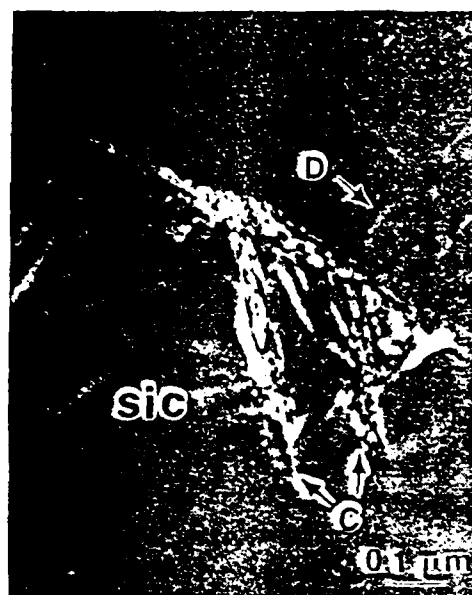


Fig. 10b. CDF image from the same region as in fig. 10a.

SiC (arrowed C) and θ' (Al_2Cu) in the aluminum matrix (arrowed D). These latter features were identified as θ' by the streaking in the $\langle 001 \rangle$ matrix directions in suitably oriented SADPs.

Figures 11a, b are a BF/ δ' CDF pair from the interfacial region. What appear to be second phase particles (arrowed on figure 11a) are located on the aluminum/ SiC interface. These particles result in a δ' PFZ, as is shown in figure 11b (the interface is arrowed). Finally, figures 12a, b are BF images from a different interface, and for different tilt

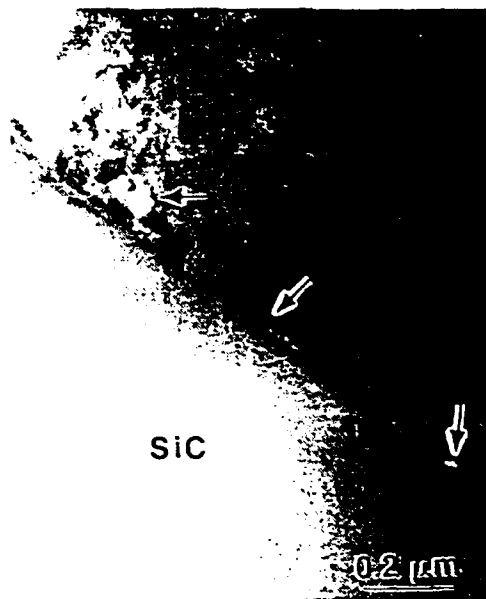


Fig. 11a. Precipitates at the matrix/SiC interface (190°C, 20hrs).

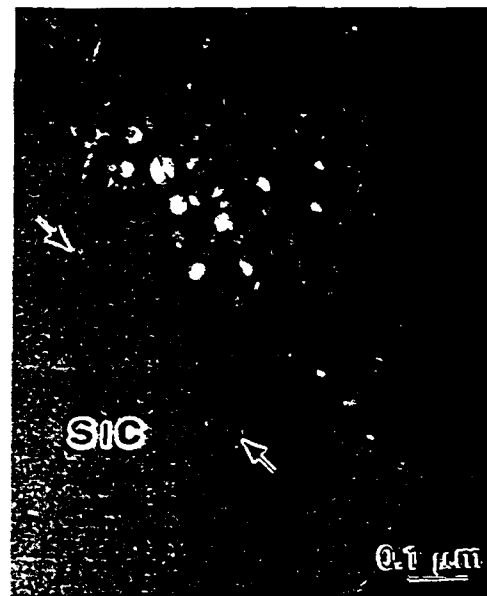


Fig. 11b. PFZ of δ' next to the interface shown in fig. 11a.

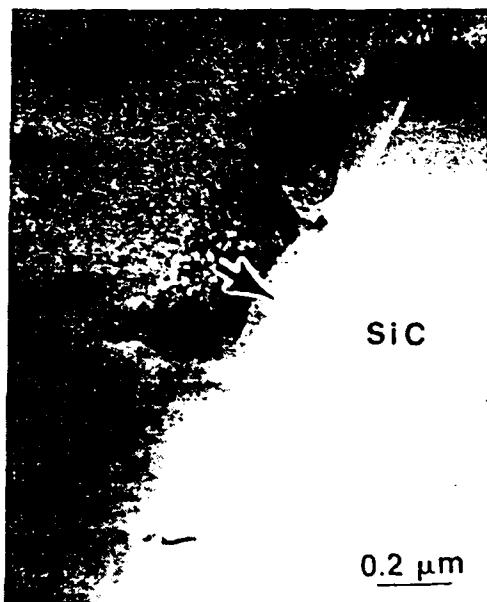


Fig. 12a. A region (arrowed) implying the presence of precipitates.



Fig. 12b. The change of tilt condition revealing the microcrystals.

conditions. In figure 12a, a region exhibiting different contrast from the matrix (arrowed) appears to be associated with the interface. However, the region is seen to be comprised of several microcrystals as shown in figure 12b. As argued in the next section, the interfacial precipitates are the T_2 phase.

DISCUSSION

The three major findings of the present investigation are:

- i) a two-stage strengthening behavior for both the control alloy and the composite;
- ii) little difference in the aging kinetics between the control alloy and the composite;
- iii) δ' PFZs within the matrix, at grain boundaries and at aluminum/SiC interfaces.

Concerning point (i), it is likely that the δ' precipitates are the main strengthening precipitate after 8 hours aging. Continued aging leads to an increase in δ' particle size, which accounts for the drop in matrix hardness after approximately 10 hours. The second hardness peak would then be associated with the precipitation, primarily of S'. This discussion is consistent with an earlier investigation of the two stage strengthening behavior of an Al-Li-Cu-Mg-Zr alloy [1] and the observation of a hardness plateau by Welpmann et al. [2].

The second point, that aging is not accelerated in the composite, is at variance with the work of e.g., Christman and Suresh [3] who showed that S' precipitation occurred more rapidly in a 2124 aluminum alloy-SiC composite, than in a control alloy, due to the high dislocation density generated during cooling from the solution treatment temperature. These dislocations were created due to mismatches in thermal expansion coefficients between aluminum and silicon carbide [3,4]. Indeed high dislocation densities were frequently observed in the present study (e.g., see figures 8c and 10a); however, accelerated aging was not observed. At present, the reason(s) for this apparent discrepancy are being explored.

The nature of the matrix/SiC interfacial regions is intriguing. For example, δ' PFZs (figure 11b) and DFZs (figure 10a) were observed, as were "microcrystalline" particles at the interface itself (figures 11a and 12a, b). These three observations can be rationalized assuming that the interfacial particles are T_2 (Al_6CuLi_3) in that a δ' (Al_3Li) PFZ would be produced automatically, and in the absence of δ' , the dislocations in the PFZ could annihilate at the matrix/SiC interface. In light of the fact that T_2 is unstable when irradiated by e.g., an electron beam [5,6], and decomposes to a microcrystalline array, it is safe to conclude that the interfacial precipitates are indeed T_2 .

CONCLUSIONS

A preliminary examination of a spray formed Al-Li/SiC composite has shown that:

- a) there is a two-stage strengthening reaction. The first peak is associated with δ' (Al_2Li); the second with S' (Al_2CuMg);
- b) the aging kinetics of the composite are not accelerated when compared with the control alloy, even though many regions of the matrix in the composite are highly dislocated;
- c) T_2 (Al_6CuLi) precipitate on the matrix/SiC interface. This leads to both precipitate and dislocation free zones.

ACKNOWLEDGMENTS

The authors are grateful to the Office of Naval Research, Grant No. N00014-91-J-1648 for financial support and for the provision of specimen material.

REFERENCES

- [1] Song, S., Zhang, W., Cheng, J., Ryba, E. R. and Howell, P. R. *Materials Letters*, **9** (1990) 430.

- [2] Welpmann, K., Peters, M. and Sanders, T. H. in: Proceedings of the 3rd International Conference on Aluminum Alloys, eds. C. Baker, P. J. Gregson, S. J. Harris and C. J. Peel, The Institute of Metals, London (1986), p. 525.
- [3] Christman, T. and Suresh, S., *Acta Metall.*, **36**, (1988) 1691.
- [4] Mahon, G. J., Howe, J. M. and Vasudevan, A. K., *Acta Metall.* **38** (1990) 1503.
- [5] Howell, P. R., Michel, D. J. and Reed, J. R., *Scripta Metall.* **24**, (1990) 1033.
- [6] Howell, P. R., Michel, D. J. and Ryba, E. R., *Scripta Metall.*, **23**, (1989) 825.

APPENDIX III

The Nucleation of T2 on the SiC/Matrix Interface in an 8090/SiC Composite

Note: This is an Abridged version of a manuscript to be submitted to Scripta Met.et Mat

Using classic nucleation theory, the ratio of the energy barrier for nucleation of T2 on an spherical particles SiC (ΔG^*) to that for homogeneous nucleation (ΔG_{hu}^*) can be calculated, as a function of SiC radius(R) to yield the curve shown in figure 1. Note that as $R \rightarrow \infty$, $\Delta G^* / \Delta G_{hu}^* \rightarrow 0.5$. In addition, as $R \rightarrow 0$, $\Delta G^* / \Delta G_{hu}^* \rightarrow 1$ (the major assumption in generating figure 1 is that the SiC/matrix interfacial free energy is equal to the SiC/T2 interfacial free energy). Now, reference to SEM images of the composite shows that many of the SiC/matrix interfaces are planar (i.e., $R=\infty$) and hence the required geometry is that shown in figure 2 and $\Delta G^* = 0.5 \Delta G_{hu}^*$. If we now turn our attention to nucleation at high angle boundaries, figure 3, and make the simplifying assumption of equality of all interfacial energies, then $\theta=30^\circ$ and $\Delta G^* \approx 0.3 \Delta G_{hu}^*$. The exact value is shown as the dotted line on figure 1. Hence, we would predict that both grain boundaries and SiC/matrix interfaces should be potent nucleation site for T2 in these composites.

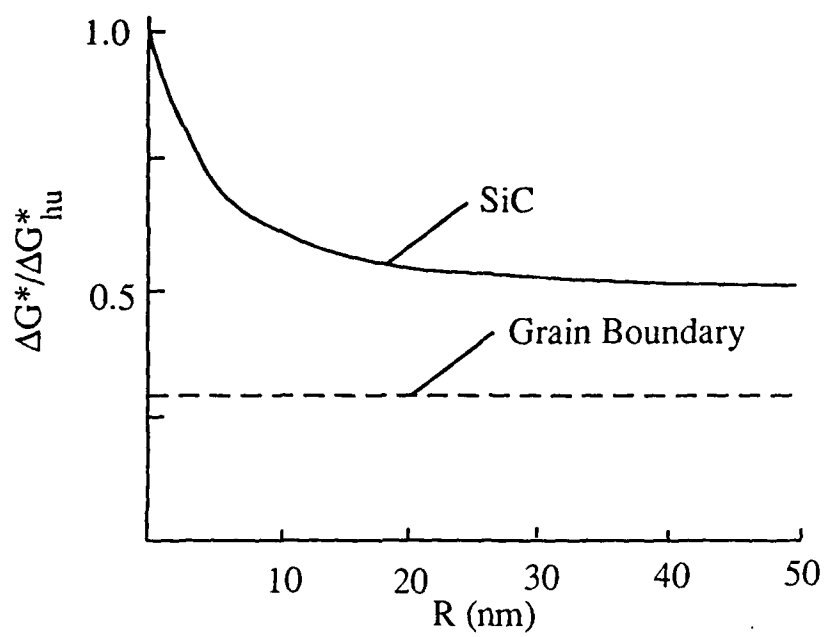
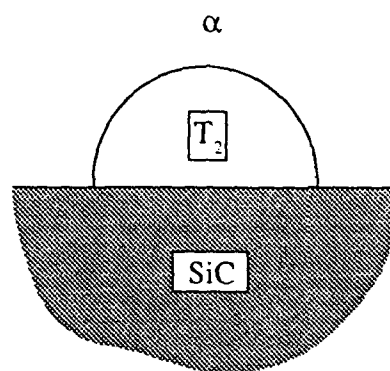
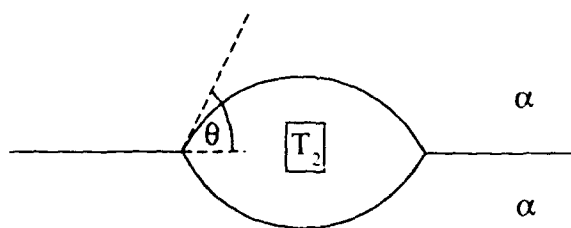


Figure 1



$$\Delta G^* = 0.5\Delta G^*_{hu}$$

Figure 2



$$\Delta G^* = \Delta G^*_{hu} 2f(\theta)$$

Figure 3